

# Theory of Raman scattering on electron-doped high- $T_c$ superconductor

C. S. Liu,<sup>1,2</sup> H. G. Luo,<sup>1</sup> W. C. Wu,<sup>2</sup> and T. Xiang<sup>1,3</sup>

<sup>1</sup>*Institute of Theoretical Physics and Interdisciplinary Center of Theoretical Studies, Chinese Academy of Sciences, P. O. Box 2735, Beijing 100080, China*

<sup>2</sup>*Department of Physics, National Taiwan Normal University, Taipei 11650, Taiwan*

<sup>3</sup>*Center for Advanced Study, Tsinghua University, Beijing 100084, China*

We have analyzed the  $B_{1g}$  and  $B_{2g}$  Raman spectra of electron-doped cuprate superconductors  $\text{Nd}_{2-x}\text{Ce}_x\text{CuO}_4$  and  $\text{Pr}_{2-x}\text{Ce}_x\text{CuO}_4$  using a weakly coupled two-band model. One of these two bands is centered around  $(\pm\pi/2, \pm\pi/2)$  and couples more strongly with the  $B_{2g}$  mode, while the other is centered around  $(\pm\pi, 0)$  and  $(0, \pm\pi)$  and couples more strongly with the  $B_{1g}$  mode. This model explains in a natural way why the  $B_{2g}$  Raman peak occurs at a higher frequency than the  $B_{1g}$  one at optimal doping, and how these two peaks change with doping in agreement with experiments. Our result suggests that the superconducting pairing in electron-doped high- $T_c$  cuprates has the  $d_{x^2-y^2}$ -wave symmetry and results from the same mechanism as for hole doped materials.

PACS numbers: 74.20.Rp, 74.20.Mn, 74.25.Nf 78.30.-j

Pairing symmetry of electron-doped high- $T_c$  cuprate superconductors such as  $\text{Nd}_{2-x}\text{Ce}_x\text{CuO}_4$  and  $\text{Pr}_{2-x}\text{Ce}_x\text{CuO}_4$  is a long standing problem [1, 2, 3, 4, 5, 6, 7, 8, 9, 10, 11, 12, 13, 14, 15, 16, 17]. Although no consensus has been reached yet, more and more recent experimental results have suggested that the order parameter of electron-doped cuprates is likely to have  $d_{x^2-y^2}$ -wave pairing symmetry [1, 2, 3, 5, 9, 10, 14, 16, 17], in close resemblance to that of hole-doped materials. Among various experiments, the Raman scattering seems to suggest a different story [13, 14, 15]. For hole-doped superconductors, it was known that typical  $B_{1g}$ ,  $B_{2g}$  and  $A_{1g}$  pair-breaking peaks appear respectively at the frequencies of 2, 1.6, and 1.2 times of the gap amplitude [18]. However, in electron-doped materials the relative position of the  $B_{1g}$  and  $B_{2g}$  peaks changes with doping. The  $B_{2g}$  peak appears first at a higher frequency than the  $B_{1g}$  one in the underdoped regime. It then moves down and finally appears at a frequency lower than that of the  $B_{1g}$  peak in the heavily overdoped regime.

The Raman scattering has the potential to probe different regions of the Fermi surface (FS), thus a thorough understanding of the experimental data can provide a better understanding on the momentum dependence of superconducting (SC) pairing gap. The observation of  $B_{2g}$  Raman peak at higher frequency than that of  $B_{1g}$  would imply a non-monotonic  $d_{x^2-y^2}$ -wave order parameter in a single-band system [14]. This non-monotonic order parameter seems to be also consistent with the observation of angle resolved photoemission spectroscopy (ARPES) [16]. However, this one-band picture may not be adequate to describe the nature of two kinds of charge carriers in electron-doped cuprate superconductors, as revealed by magneto-transport measurements [19, 20, 21].

A key clue towards the understanding of Raman data in  $\text{Nd}_{2-x}\text{Ce}_x\text{CuO}_4$  comes from the doping evolution of the FS revealed by ARPES [22, 23]. At low doping, four small FS pockets first appear around  $(\pm\pi, 0)$  and  $(0, \pm\pi)$ . By increasing the doping, four new pockets begin to form

around  $(\pm\pi/2, \pm\pi/2)$ . These results can be explained in terms of the  $\mathbf{k}$ -dependent band-folding effect due to antiferromagnetic (AF) ordering. The original band is folded back into the magnetic Brillouin zone (MBZ) around the diagonal line  $(\pi, 0) \rightarrow (0, \pi)$ . Near the intersecting points of the Fermi surface, an AF gap opens and splits the original FS into two [24, 25, 26]. This two-band picture was first used by Luo and Xiang to explain the unusual temperature dependence of the magnetic penetration depth in electron-doped copper oxides [27]. It is supported by Hall coefficient and magneto-resistance measurements [19, 20, 21]. The generic feature of a weakly coupled two-band model was discussed in Ref. [28] in the context of hole-doped cuprate superconductors.

In this Letter, we shall use a two-band model to study the Raman response for the electron-doped cuprates. As will be shown, the two-band model gives a unified explanation to the unusual behaviors of Raman spectra. It explains in a natural way why the  $B_{2g}$  Raman peak appears at a higher frequency than that of the  $B_{1g}$  peak at optimal doping and why the relative positions of these two peaks change in the heavily overdoped regime.

We start by considering the two-dimensional  $t$ - $t'$ - $t''$ - $J$  model

$$H = -t \sum_{\langle ij \rangle_{1\sigma}} c_{i\sigma}^\dagger c_{j\sigma} - t' \sum_{\langle ij \rangle_{2\sigma}} c_{i\sigma}^\dagger c_{j\sigma} - t'' \sum_{\langle ij \rangle_{3\sigma}} c_{i\sigma}^\dagger c_{j\sigma} + J \sum_{\langle ij \rangle} (\vec{S}_i \cdot \vec{S}_j - \frac{1}{4} n_i n_j), \quad (1)$$

where  $\langle ij \rangle_1$ ,  $\langle ij \rangle_2$ , and  $\langle ij \rangle_3$  denote the nearest, second-nearest, and third-nearest neighbors between  $i$  and  $j$ . All notations used in (1) are standard. Applying the mean-field approximation [25], Hamiltonian (1) can be transformed and written in terms of two (diagonalized) bands in momentum space

$$H = \sum_{\mathbf{k}\sigma} (\xi_{\mathbf{k}\alpha} \alpha_{\mathbf{k}\sigma}^\dagger \alpha_{\mathbf{k}\sigma} + \xi_{\mathbf{k}\beta} \beta_{\mathbf{k}\sigma}^\dagger \beta_{\mathbf{k}\sigma}), \quad (2)$$

where the prime denotes that the momentum summation is over the MBZ only ( $-\pi < k_x \pm k_y \leq \pi$ ),

$$\xi_{\mathbf{k},l} = \frac{\varepsilon_{\mathbf{k}} + \varepsilon_{\mathbf{k}+\mathbf{Q}}}{2} \mp \sqrt{\frac{(\varepsilon_{\mathbf{k}+\mathbf{Q}} - \varepsilon_{\mathbf{k}})^2}{4} + 4J^2m^2}, \quad (3)$$

$m$  is the AF order and

$$\varepsilon_{\mathbf{k}} = (2|t|\delta - J\chi)(\cos k_x + \cos k_y) - 4t'\delta \cos k_x \cos k_y - 2t''\delta(\cos 2k_x + \cos 2k_y) \quad (4)$$

with  $\chi$  the uniform bond order and  $\delta$  the doping concentration.

In the SC state, we add a BCS coupling term to each band and assume the system to be described by the following Hamiltonian [27]

$$H = \sum_{\mathbf{k}\sigma l} \xi_{\mathbf{k}l} l_{\mathbf{k}\sigma}^\dagger l_{\mathbf{k}\sigma} + \Delta_{\mathbf{k}l} (l_{\mathbf{k}\uparrow}^\dagger l_{-\mathbf{k}\downarrow}^\dagger + l_{-\mathbf{k}\uparrow} l_{\mathbf{k}\downarrow}), \quad (5)$$

where  $l \equiv \alpha, \beta$  and  $\Delta_{\mathbf{k}l} = \Delta_l[\cos k_x - \cos k_y]$  are the  $d_{x^2-y^2}$ -wave gap functions.

The Raman scattering intensity is proportional to the imaginary part of the effective density-density correlation function  $\chi(\mathbf{q}, \tau) = \langle T_\tau [\tilde{\rho}(\mathbf{q}, \tau), \tilde{\rho}(-\mathbf{q}, 0)] \rangle$  in the limit  $\mathbf{q} \rightarrow 0$ . Here  $\tilde{\rho}(\mathbf{q}, \tau) \equiv \sum_{\mathbf{k}, \sigma} \gamma_{\mathbf{k}} c_{\mathbf{k}+\mathbf{q}/2}^\dagger(\tau) c_{\mathbf{k}-\mathbf{q}/2}(\tau)$  is the effective density operator and  $\gamma_{\mathbf{k}}$  is the Raman vertex. When the energy of incident light is smaller than the optical band gap, the contribution from the resonance channel is negligible. The Raman vertex can then be obtained in terms of the curvature of the band dispersion under the inverse effective mass approximation.

From the linear response theory, it can be shown that the Raman response function for each symmetric channel (S) is given by

$$\chi^S(\mathbf{q} \rightarrow 0, \tau) = - \sum_{\mathbf{k}, l, l'} (\gamma_{\mathbf{k}, ll'}^S)^2 [\mathcal{G}_l(\mathbf{k}, \tau) \mathcal{G}_{l'}(\mathbf{k}, -\tau) - \epsilon_{ll'} \mathcal{F}_l(\mathbf{k}, \tau) \mathcal{F}_{l'}(\mathbf{k}, -\tau)], \quad (6)$$

where  $\mathcal{G}$  and  $\mathcal{F}$  are the normal and anomalous Green functions for a superconductor,  $\epsilon_{ll'} = 1$  if  $l = l'$  or  $-1$  if  $l \neq l'$ . The intra- and interband vertex functions are

$$\begin{aligned} \gamma_{\mathbf{k}, \alpha\alpha}^S &= \cos^2 \theta_{\mathbf{k}} \gamma_{\mathbf{k}}^S + \sin^2 \theta_{\mathbf{k}} \gamma_{\mathbf{k}+\mathbf{Q}}^S, \\ \gamma_{\mathbf{k}, \beta\beta}^S &= \sin^2 \theta_{\mathbf{k}} \gamma_{\mathbf{k}}^S + \cos^2 \theta_{\mathbf{k}} \gamma_{\mathbf{k}+\mathbf{Q}}^S, \\ \gamma_{\mathbf{k}, \alpha\beta}^S &= \gamma_{\mathbf{k}, \beta\alpha}^S = \sin 2\theta_{\mathbf{k}} (\gamma_{\mathbf{k}}^S - \gamma_{\mathbf{k}+\mathbf{Q}}^S), \end{aligned} \quad (7)$$

where  $\cos 2\theta_{\mathbf{k}} \equiv (\varepsilon_{\mathbf{k}+\mathbf{Q}} - \varepsilon_{\mathbf{k}}) / \sqrt{(\varepsilon_{\mathbf{k}+\mathbf{Q}} - \varepsilon_{\mathbf{k}})^2 + 4J^2m^2}$ . For the  $B_{1g}$  and  $B_{2g}$  channels,  $\gamma_{\mathbf{k}}^{B_{1g}} = \gamma_{\mathbf{k}}^{xx} - \gamma_{\mathbf{k}}^{yy}$  and  $\gamma_{\mathbf{k}}^{B_{2g}} = 2\gamma_{\mathbf{k}}^{xy}$ . Here  $\gamma_{\mathbf{k}}^{ij} \equiv \partial^2 \varepsilon_{\mathbf{k}} / \partial k_i \partial k_j$  (inverse effective mass approximation).

Shown in Fig. 1 are the  $B_{2g}$  and  $B_{1g}$  Raman vertices and how they are coupled to the SC quasiparticle excitations in  $\mathbf{k}$  space. Since the  $B_{2g}$  vertex has  $d_{xy}$  symmetry, the  $B_{2g}$  channel is dominated by the excitations of the  $\beta$  band. In contrast, the  $B_{1g}$  vertex has  $d_{x^2-y^2}$  symmetry,

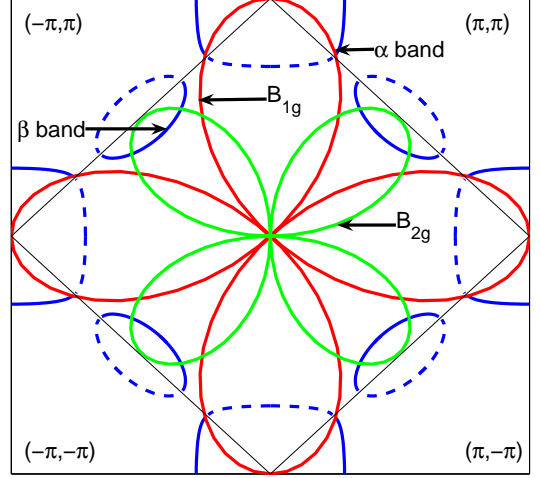


FIG. 1: Schematic plot of the Fermi surfaces for the  $\alpha$  and  $\beta$  bands and the momentum dependence of the  $B_{1g}$  and  $B_{2g}$  Raman vertices. The  $B_{1g}$  and  $B_{2g}$  modes couple more strongly with the  $\alpha$  and  $\beta$  bands, respectively.

thus the  $B_{1g}$  channel is contributed mainly from the excitations of the  $\alpha$  band. Since both  $B_{2g}$  and  $B_{1g}$  vertices are odd-parity, their Raman intensities are not affected by the Coulomb screening. For the fully symmetric  $A_{1g}$  channel, in contrast, all regions of momentum space contribute and the Raman intensity is partially screened. Since the  $A_{1g}$  channel is more sensitive to the screening effect, we will leave out  $A_{1g}$  and focus on the  $B_{2g}$  and  $B_{1g}$  channels only.

In electron doped cuprates, the SC state appears only when the  $\beta$  band emerges above the Fermi energy. This would suggest us to assume that it is the  $\beta$  band that drives the system to superconduct, while the  $\alpha$  band becomes superconducting mainly via the proximity effect. A simple picture for the understanding of the unusual Raman spectra in electron doped cuprates can then be sketched as follows. In the under- or optimally doped regime, the  $\beta$ -band couples more strongly with the AF fluctuations than the  $\alpha$  band. This results in a relatively larger SC gap in the  $\beta$  band ( $\Delta_\beta$ ) than in the  $\alpha$  band ( $\Delta_\alpha$ ). The  $B_{1g}$  channel probes mainly the quasi-particle (QP) excitations of the  $\alpha$  band, thus the  $B_{1g}$  Raman peak is mainly determined by  $\Delta_\alpha$ . Similarly, the  $B_{2g}$  channel probes mainly the QP excitations of the  $\beta$  band, its Raman peak is mainly determined by  $\Delta_\beta$ . If  $\Delta_\alpha$  is much smaller than  $\Delta_\beta$ , one would then expect that the  $B_{1g}$  peak appears at a frequency lower than that of the  $B_{2g}$  peak, unlike in the hole doped case. In the heavily overdoped regime, the AF correlation becomes very weak and the band splitting vanishes. In this case the two-band model reduces essentially to a one-band model and the  $B_{1g}$  and  $B_{2g}$  Raman spectra would behave similarly as in the hole doped cuprate superconductors, consistent with the experiments.

Pertaining to  $\text{Nd}_{2-x}\text{Ce}_x\text{CuO}_4$ , we have adopted  $|t| = 0.326eV$ ,  $t' = 0.3t$ ,  $t'' = -0.2t$ , and  $J = 0.3t$  to sim-

ulate the band structure [25]. To be consistent with the self-consistent calculations, we take  $\chi = -0.15$  and  $m = 0.178$  for the optimally-doped ( $x = 0.15$ ) sample,  $\chi = -0.15$  and  $m = 0.15$  for the overdoped ( $x = 0.16$ ) sample. The chemical potentials are determined by the filling factor for each band to give the true doping concentration through  $x = n_e - n_h$ .

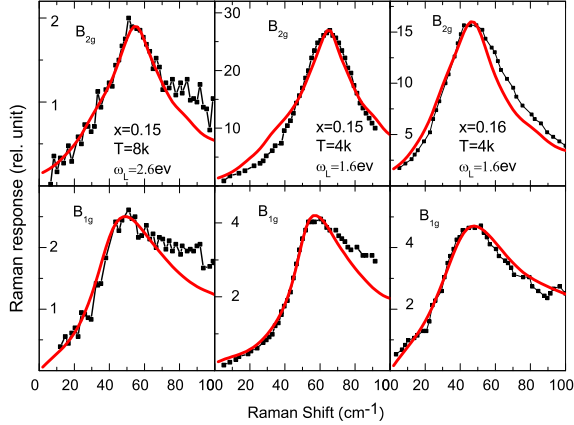


FIG. 2: Comparison of the theoretical calculations (solid lines) with the measurement data (dotted lines) for  $\text{Nd}_{2-x}\text{Ce}_x\text{CuO}_4$ . The experimental data in the first column are taken from Ref. [14]. The data in the second and third columns are taken from Ref.[15].  $\omega_L$  is the incident photon energy.

Theoretical fitting procedures are implemented as follows. First, the vertex functions are evaluated using (7). Then the SC gaps  $\Delta_\alpha$  and  $\Delta_\beta$  and the smearing Lorentz width  $\Gamma_\alpha$  and  $\Gamma_\beta$  are adjusted to fit the peak positions and the overall spectral lineshape (up to a constant multiplying factor).

Fig. 2 compares the experimental data of Raman spectra for  $\text{Nd}_{2-x}\text{Ce}_x\text{CuO}_4$  with the theoretical calculations. For all the cases considered in Fig. 2, our fitting curves are in good agreement with the experimental results. For the optimally doped sample ( $x=0.15$ ) reported in Ref. [14] at  $T = 8\text{K}$  (first column), the  $B_{1g}$  and  $B_{2g}$  Raman peaks appear at  $50\text{cm}^{-1}$  and  $55\text{cm}^{-1}$ , respectively. The corresponding gap and smearing parameters obtained by fitting are  $(\Delta_\alpha, \Delta_\beta) = (21\text{cm}^{-1}, 48\text{cm}^{-1})$  and  $(\Gamma_\alpha, \Gamma_\beta) = (6\text{cm}^{-1}, 8\text{cm}^{-1})$ . The ratio between the  $B_{1g}$  Raman peak frequency and  $\Delta_\alpha$  is about 2.4, while the ratio between the  $B_{2g}$  Raman peak frequency and  $\Delta_\beta$  is about 1.2. The corresponding ratios in a hole doped  $d_{x^2-y^2}$ -wave superconductor are about 2 and 1.6, respectively. This difference between hole and electron doped cuprates is not difficult to be understood. In electron doped materials, the AF correlation splits the continuous FS into two separate sheets. This then suppresses the high (low) energy region to which the  $B_{2g}$  ( $B_{1g}$ ) probes. It is thus expected that the  $B_{2g}$  ( $B_{1g}$ ) peak will be red-

shifted (blue-shifted) compared with the result of hole-doped cuprate superconductors.

For another set of data of the optimally doped sample reported in Ref. [15] at  $T = 4\text{K}$  (second column), the fitting parameters are  $(\Delta_\alpha, \Delta_\beta) = (27\text{cm}^{-1}, 57\text{cm}^{-1})$  and  $(\Gamma_\alpha, \Gamma_\beta) = (4\text{cm}^{-1}, 6\text{cm}^{-1})$ . The corresponding parameters for the overdoped sample at  $T = 4\text{K}$  (third column) are  $(\Delta_\alpha, \Delta_\beta) = (21\text{cm}^{-1}, 37\text{cm}^{-1})$  and  $\Gamma_\alpha = \Gamma_\beta = 8\text{cm}^{-1}$ . The gap parameters above obtained are consistent with the general expectation. Both  $\Delta_\alpha$  and  $\Delta_\beta$  decrease with increasing temperature at the same doping level and with increasing doping at the same temperature. The gap ratio,  $r \equiv \Delta_\beta/\Delta_\alpha$ , is reduced from 2 at optimal doping to 1.7 at slightly overdoping, consistent with the scenario of AF-like fluctuation induced superconductivity.

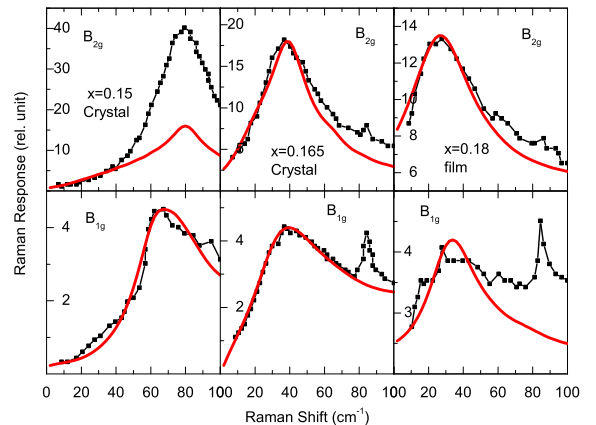


FIG. 3: Comparison between the theoretical results (solid curves) and the Raman measurement data from Ref. [15] (dotted curves) for  $\text{Pr}_{2-x}\text{Ce}_x\text{CuO}_4$  at  $T = 4\text{K}$ .  $\omega_L = 1.9\text{eV}$ .

The Raman scattering measurement has also been carried out in electron-doped  $\text{Pr}_{2-x}\text{Ce}_x\text{CuO}_4$  at various doping levels[15]. The Raman spectra of  $\text{Pr}_{2-x}\text{Ce}_x\text{CuO}_4$ , as shown in Fig. 3, behave similarly as for  $\text{Nd}_{2-x}\text{Ce}_x\text{CuO}_4$ . At optimal doping, the  $B_{2g}$  peak appears at a frequency higher than that of the  $B_{1g}$  peak. With increasing doping, the frequency of the  $B_{1g}$  peak approaches to and finally surpasses the  $B_{2g}$  peak in the overdoped regime.

Fig. 3 compares the measurement data of  $\text{Pr}_{2-x}\text{Ce}_x\text{CuO}_4$  with our theoretical calculations. For the optimally-doped sample ( $x = 0.15$ ), the Raman peak appears at  $80\text{cm}^{-1}$  for the  $B_{2g}$  mode and at  $62\text{cm}^{-1}$  for the  $B_{1g}$  mode. The parameters obtained by fitting are  $(\Delta_\alpha, \Delta_\beta) = (31\text{cm}^{-1}, 68\text{cm}^{-1})$  and  $\Gamma_\alpha = \Gamma_\beta = 6\text{cm}^{-1}$ , with  $\chi = -0.15$ , and  $m = 0.15$ . For the slightly overdoped sample ( $x = 0.165$ ), the  $B_{2g}$  and  $B_{1g}$  peaks appear at the same frequency at  $37\text{cm}^{-1}$  and the parameters we obtained are  $(\Delta_\alpha, \Delta_\beta) = (16\text{cm}^{-1}, 30\text{cm}^{-1})$ ,  $\Gamma_\alpha = \Gamma_\beta = 8\text{cm}^{-1}$ ,  $\chi = -0.15$  and  $m = 0.12$ . For

the heavily over-doped sample ( $x = 0.18$ ), the Raman peaks appear at  $25 \text{ cm}^{-1}$  and  $30 \text{ cm}^{-1}$  for the  $B_{2g}$  and  $B_{1g}$  modes, respectively. The relative peak positions of these two modes are similar as in a one-band  $d_{x^2-y^2}$ -wave superconductor. This is not unexpected since at such a high doping level, the two-band model reduces essentially to a one-band model. In this case, the parameters we obtained are  $\Delta_\alpha = \Delta_\beta = 15 \text{ cm}^{-1}$ ,  $\Gamma_\alpha = \Gamma_\beta = 15 \text{ cm}^{-1}$ ,  $\chi = -0.15$  and  $m = 0$ . For the above three samples, the ratio  $\Delta_\beta/\Delta_\alpha$  changes from 2.3, to 1.9, and finally to 1 with increasing doping.

In the top-left panel of Fig. 3 for the  $B_{2g}$  mode, the experimental data are taken under the strong *resonant* regime as emphasized in Refs. [14, 15]. In this case, the contribution from the resonance channel becomes important and the inverse effective mass approximation is not valid. Our theoretical result including only the non-resonant contribution can give a good explanation to the low-frequency part of the spectrum, but the height of the peak is much lower than the experimental one. The res-

onance channel may also have some contribution to the  $B_{2g}$  spectrum in the second column of Fig. 2 for  $\text{Nd}_{2-x}\text{Ce}_x\text{CuO}_4$ .

In conclusion, we have analyzed the Raman spectra of electron-doped cuprate superconductors based on a weakly coupled two-band model. Our result gives a unified explanation to the experimental data in the whole doping range. It suggests strongly that the SC pairing in electron-doped cuprate superconductors results from the same pairing mechanism as in hole doped ones and the gap parameter has  $d_{x^2-y^2}$ -wave symmetry. To understand the Raman data in the strong resonance regime, a more comprehensive theory including the contribution from the resonance channel is desired.

We are grateful to Hsiang-Lin Liu for useful comments on Raman experiments. This work was supported by the National Natural Science Foundation of China (Grant No. 10347149), National Basic Research Program of China (Grant No. 2005CB32170X), and National Science Council of Taiwan (Grant No. 93-2112-M-003-015).

- 
- [1] C. Tsuei and J. R. Kirtley, Phys. Rev. Lett. **85**, 182 (2000).
- [2] N. P. Armitage, D. H. Lu, D. L. Feng, C. Kim, A. Damascelli, K. M. Shen, F. Ronning, Z.-X. Shen, Y. Onose, Y. Taguchi, et al., Phys. Rev. Lett. **86**, 1126 (2001).
- [3] T. Sato, T. Kamiyama, T. Takahashi, K. Kurahashi, and K. Yamada, Science **291**, 1517 (2001).
- [4] L. Alff, S. Meyer, S. Kleefisch, U. Schoop, A. Marx, H. Sato, M. Naito, and R. Gross, Phys. Rev. Lett. **83**, 2644 (1999).
- [5] R. Prozorov, R. Giannetta, P. Fourier, and R. Greene, Phys. Rev. Lett. **85**, 3700 (2000).
- [6] J. A. Skinta, M.-S. Kim, T. R. Lemberger, T. Greibe, and M. Naito, Phys. Rev. Lett. **88**, 207005 (2002).
- [7] M.-S. Kim, J. A. Skinta, T. R. Lemberger, A. Tsukada, and M. Naito, Phys. Rev. Lett. **91**, 087001 (2003).
- [8] A. Biswas, P. Fournier, M. Qazilbash, V. Smolyaninova, H. Balci, and R. Greene, Phys. Rev. Lett. **88**, 207004 (2002).
- [9] B. Chesca, K. Ehrhardt, Mössle, R. Straub, D. Kollé, R. Kleiner, and A. Tsukada, Phys. Rev. Lett. **90**, 057004 (2003).
- [10] B. Chesca, M. Seifried, T. Dahm, N. Schopohl, D. Koelle, R. Kleiner, and A. Tsukada, Phys. Rev. B **71**, 104504 (2005).
- [11] L. Shan, Y. Huang, H. Gao, Y. Wang, S. L. Li, P. C. Dai, F. Zhou, J. W. Xiong, W. X. Ti, and H. H. Wen, Phys. Rev. B **72**, 144506 (2005).
- [12] H. Balci and R. L. Greene, Phys. Rev. Lett. **93**, 067001 (2004).
- [13] B. Stadlober, G. Krug, R. Nemetschek, R. Hackl, J. L. Cobb, and J. T. Markert, Phys. Rev. Lett. **74**, 4911 (1995).
- [14] G. Blumberg, A. Koitzsch, A. Gozar, B. Dennis, C. Kendziora, P. Fourier, and R. L. Greene, Phys. Rev. Lett. **88**, 107002 (2002).
- [15] M. M. Qazilbash, B.S. Dennis, C. A. Kendziora, H. Balci, R. L. Greene, and G. Blumberg, cond-mat/0501362; M. M. Qazilbash, A. Koitzsch, B. S. Dennis, A. Gozar, H. Balci, C. A. Kendziora, R. L. Greene, and G. Blumberg, cond-mat/0510098.
- [16] H. Matsui, K. Terashima, T. Sato, T. Takahashi, M. Fujita, and K. Yamada, Phys. Rev. Lett. **95**, 017003 (2005).
- [17] Ariando, D. Darminto, H. J. H. Smilde, V. Leca, D. H. A. Blank, H. Rogalla, and H. Hilgenkamp, Phys. Rev. Lett. **94**, 167001 (2005).
- [18] T. P. Devereaux and D. Einzel, Phys. Rev. B **51**, 16336 (1995).
- [19] Z. Z. Wang, T. R. Chien, and N. P. Ong, Phys. Rev. B **43**, 3020 (1991).
- [20] W. Jiang, S. N. Mao, X. X. Xi, X. Jiang, J. L. Peng, T. Venkatesan, C. J. Lobb, and R. L. Greene, Phys. Rev. Lett. **73**, 1291 (1994).
- [21] P. Fournier, X. Jiang, W. Jiang, S. N. Mao, C. J. L. T. Venkatesan, and R. L. Greene, Phys. Rev. B **56**, 14149 (1997).
- [22] N. P. Armitage, F. Ronning, D. H. Lu, C. Kim, A. Damascelli, K. M. Shen, D. L. Feng, H. Eisaki, Z. X. Shen, P. K. Mang, et al., Phys. Rev. Lett. **88**, 257001 (2002).
- [23] H. Matsui, K. Terashima, T. Sato, T. Takahashi, S.-C. Wang, H.-B. Yang, H. Ding, T. Uefuji, and K. Yamada, Phys. Rev. Lett. **94**, 047005 (2005).
- [24] C. Kusko, R. S. Markiewicz, M. Lindroos, and A. Bansil, Phys. Rev. B **66**, 140513 (2002).
- [25] Q. Yuan, Y. Chen, T. K. Lee, and C. S. Ting, Phys. Rev. B **69**, 214523 (2004).
- [26] K. K. Voo and W. C. Wu, Physica C **417**, 103 (2005).
- [27] H. G. Luo and T. Xiang, Phys. Rev. Lett. **94**, 027001 (2005).
- [28] T. Xiang and J. M. Wheatley, Phys. Rev. Lett. **76**, 134 (1996).